Measurements of Singly Ionized Atomic Iodine Hyperfine Coupling Coefficients Using Intermodulated Laser Induced Fluorescence

M. J. Lazo[1], T. E. Steinberger[1], T. M. Good[2], E. E. Scime[1]

[1]West Virginia University, Department of Physics & Astronomy, Morgantown, WV 26506
[2]Gettysburg College, Department of Physics & Astronomy, Gettysburg, PA 17325

E-mail: matthewjlazo@gmail.com

Abstract. Electrostatic propulsion systems widely use xenon as a propellant, however, iodine is one candidate under consideration to replace xenon due to its attractive qualities as a propellant. A key tool missing in the development of iodine-fueled propulsion systems is a spatially resolved diagnostic technique to analyze the performance of such systems without pertubring the plasma. Previous work investigated the lineshape of singly-ionized atomic iodine (I II) with laser induced fluorescence (LIF), but could not resolve the hyperfine structure of the $^5D_4^0$ and $^5P_3$ states [*Steinberger and Scime*, Journal of Propulsion and Power, 34, 2018]. Here, an intermodulated LIF technique is used to measure a Doppler-reduced lineshape of the same I II transitions. A Monte Carlo fitting algorithm is used to fit the transition lineshape, where the magnetic dipole and electric quadrupole coupling coefficients are left as free parameters with constraints from theory. We report most probable values of the hyperfine coupling coefficients.

1. Introduction

Hall thrusters are one widely used electric propulsion device in modern spacecraft designs, mostly implemented for spacecraft orbit control.[1] They function by crossing an axial electric field with a radial magnetic field, confining electrons to orbit about the center of the device. Confined electrons ionize the neutral injected fuel, and these newly-created ions are efficiently accelerated out of the device, creating thrust.[2]

Practical propellants have large atomic mass, low ionizaion potential, are inert, and are easily stored. Xenon (Xe) is the current industry standard for Hall thruster propellant. Bismuth (Bi), krypton (Kr), and iodine (I) are commonly cited as alternative propellant choices.[1,3–7] Table 1 lists relevant physical properties for each of these elements. Detailed comparisons between each element as a Hall thruster propellant are discussed elsewhere, and are summarized here. Bismuth is an attractive candidate because it has the lowest ionization potential and highest mass of the four elements mentioned here. However, it has been largely dismissed as a propellant due to its extremely high boiling point compared to other candidates, making on-board propellant feed systems challenging to design.[8] Krypton, being significantly cheaper than xenon

Property	Bi	I	Kr	Xe
Atomic mass (amu)	209.0	126.9	83.8	131.3
First ionization potential (eV)	7.3	10.5	14	12.1
Density at STP (mg/cm^3)	9.8	4.9	3.7*	5.9
Boiling point at STP (°C)	1564	184.4	-153.2	-108.1

Table 1: Properties of several commonly considered propellants for electric propulsion systems. *Measured at 0°C.

while sharing similar properties as a noble gas, has been tested more widely in Hall thrusters. However, it has a low storage density and mass compared to xenon, and underperformed as a propellant when compared with xenon.[5,6] Cryogenic storage has been explored as a partial solution for storage of krypton aboard spacecraft, but is not especially practical for use on small satellites.[9]

Exploratory experiments with iodine as a propellant show similar performance to xenon.[4,7,10] While atomic iodine is slightly lighter than xenon, it naturally occurs as a diatom, such that an unknown fraction of the propellant exhaust is nearly twice the mass of xenon ions. Iodine additionally has a lower ionization potential than xenon.[11,12] Furthermore, iodine can be stored easily as a solid, and transitions directly to vapor at low temperatures, making for relatively inexpensive storage solutions compared to the gas feed systems required for xenon and other propellant candidates.

Ideal evaluation of iodine-fueled electric propulsion systems requires non-perturbative plasma diagnostics with high spatial resolution that provide information about ion temperature and velocity. In this work, we provide measurements of singly-ionized atomic iodine (I II) using an intermodulated laser induced fluorescence (LIF) technique. The presence of a hyperfine structure is clear, and the intermodulated LIF technique provides an enhanced lineshape of the allowed hyperfine transitions first investigated experimentally by *Steinberger and Scime.*[13] We characterize the I II lineshape as a function of the magnetic dipole and electric quadrupole coupling coefficients. Then, a Monte Carlo fitting algorithm to the measured lineshape is performed to estimate most probable values for the coupling coefficients.

2. Laser Induced Fluorescence

LIF is a non-perturbative absorption spectroscopic technique first introduced by *Stern and Johnson.*[14] LIF uses a specific wavelength of light to excite an electronic transition of an atom or ion, commonly from a metastable state to a higher energy state. As the electron relaxes from the excited state to a lower energy state, a photon is emitted and collected as LIF signal. In a plasma, the particles will possess some random thermal motion which causes a Doppler-shift in the laboratory reference frame transition frequency. As a result, the measured lineshape is broadened around the rest absorption frequency. When the particle motion is purely thermal in nature, the

measured lineshape is a convolution of a Maxwellian lineshape (a thermal contribution) and a Lorentzian lineshape (a natural linewidth contribution). In most cases, Doppler broadening dominates the lineshape and therefore it is a suitable approximation to assume a Maxwellian lineshape. The ability of LIF to measure ion velocity distribution functions (IVDFs) makes it a viable diagnostic for non-perturbatively measuring bulk ion flow, ion temperature, and relative state density.

The LIF scheme investigated here for I II was first proposed by *Hargus et al.*,[8] who performed initial investigations with passive emission spectroscopy, and later demonstrated by *Steinberger and Scime* with LIF.[13] Laser light tuned to 696.0964 nm (vacuum) excites the metastable $^5D_4^0$ state to the $^5P_3$ upper state, which then decays to the $^5S_2^0$ state, emitting a photon of wavelength 516.264 ± 0.001 nm.[13] A partial diagram of the LIF scheme used in this work is shown in Fig. 1.

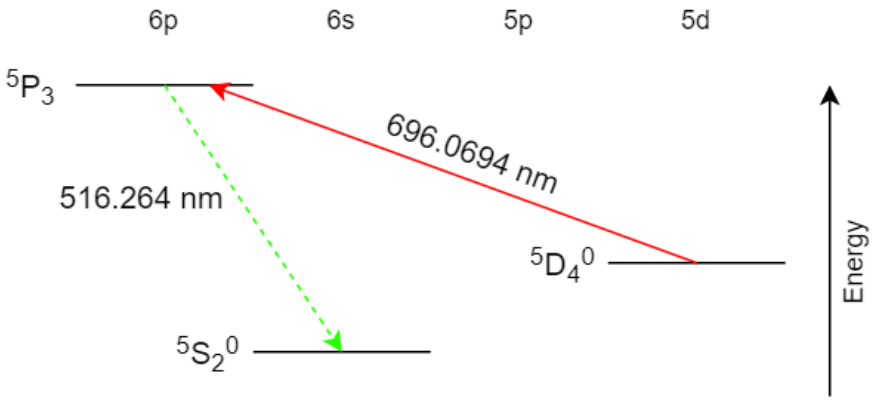

Figure 1: Partial LIF scheme for the singly ionized atomic iodine transition probed here. The pump transition to the metastable excited state is shown by the red (solid) line, and the fluorescent transition to the lower state is shown by the green (dashed) line.

2.1. Hyperfine Structure of Singly Ionized Atomic Iodine

An atom's spectrum of electronic energy levels is naturally split into a fine structure by spin-orbit coupling and relativistic corrections to bound electron orbital motion. The interactions between the nuclear magnetic dipole and electric quadrupole moments cause further, hyperfine splitting of electronic states.[15] The presence of isotopes also causes hyperfine splitting due to their unbalanced number of neutrons and protons in the nucleus. However, the only naturally-occurring isotope of iodine is I^{127}, which allows the hyperfine structure of the transition probed here to be parameterized in terms of the magnetic dipole and electric quadrupole interactions for the upper and lower states.[8,13]

When describing the hyperfine structure of an atom, it is convenient to work in the basis which couples the interactions between orbiting electrons and the nucleus. In this basis, the nuclear spin of iodine, $I = 5/2$, is added to the total electronic angular momentum J of each state, to yield the total angular momentum for each hyperfine

state, F.[13,15] Both the $^5D_4^0$ and $^5P_3$ states are split into $2I+1=6$ hyperfine states, each with a unique F, which can take on values of $F = J+I, J+I-1, ..., |J-I|$.[8]

Each hyperfine state is shifted from its unsplit state as described by

$$\Delta E/h = \Delta\nu = \frac{A}{2}C + \frac{B}{4}\frac{\frac{3}{2}C(C+1) - 2I(I+1)J(J+1)}{I(2I-1)J(2J-1)} \tag{1}$$

where h is Planck's constant, $C = F(F+1) - I(I+1) - J(J+1)$, A is the magnetic dipole coupling coefficient, and B is the electric quadrupole coupling coefficient. Following the selection rule $\Delta F = 0, \pm 1$, a model of 15 allowed transitions is created. Table 2 lists the transitions with their respective frequency shifts in terms of the coupling coefficients, as well relative intensities calculated by *Hargus et al.*[8] The numerical values of the energy shifts for each split state cannot be calculated until the coupling coefficients for the upper and lower states are known.[8] For quick reference, we label the upper state's coupling coefficients as A_U and B_U, and the lower state's coupling coefficients as A_L and B_L. These values are typically determined experimentally.

The overall lineshape for the hyperfine transitions is given by the function

$$f(\nu) = a + \sum_{i=1}^{i=15} b_i exp\left[-\gamma\frac{(\nu-\nu_{hf,i})^2}{T}\right] \tag{2}$$

where ν is the scanning frequency of the laser, in GHz, and $\gamma = \frac{mc^2}{4k\nu_0}$, with the mass m of I II in kg, the speed of light c in m/s, Boltzmann's constant k in J/K, and the rest transition frequency ν_0, in GHz. The 21 parameters of this function are: a signal offset a; scaling magnitudes, b_i, for each transition; the hyperfine transition frequencies, $\nu_{hf,i}$, in GHz, each a function of A_U, B_U, A_L, and B_L; and the source temperature, T, in eV. These are all left as free parameters for a least-squares fitting algorithm and experimental data is fit with Eq. 2 (Section 4).

2.2. Intermodulated Spectroscopy

At the scale of hyperfine structure energy shifts, Doppler broadening observed in traditional LIF results in several overlapping hyperfine transitions, which makes it difficult or impossible to resolve individual hyperfine lineshapes. This is evident from initial LIF measurements of I II, where the hyperfine structure of the measured transition is significant.[13] Therefore, an intermodulated LIF technique[16] is implemented to enhance each of the 15 hyperfine transitions probed in this work.

Intermodulated spectroscopy intersects two laser beams from the same source at a point in the plasma, with each beam modulated at a frequency which is not a harmonic of the other. LIF signal is then referenced to the sum of the two modulation frequencies. In this technique, ions at or near zero velocity interact with both beams simultaneously, amplifying the signal from particles at rest and reducing the effective Doppler width of the measured lineshape.

3. Experimental Configuration

Figure 2 shows a diagram of the experimental configuration for the measurements presented here. The plasma source is composed from crystalline iodine sealed within an Opthos Instruments Inc. quartz cell at $< 10^{-4}$ torr.[13] The cell is kept stationary, and partially inserted into an Evenson microwave resonant cavity which is driven at 2.45 GHz. Extending from the cell is a chilling finger through which an equal-parts mixture of ethylene glycol and water is circulated by a Polyscience PD07R-40 chiller that has an operating range of $-20°$ C to $100°$ C. *Kono and Hattori*[17] measured the iodine partial pressure in a similar cell configuration to be

$$\log_{10}(P) = 18.8 - 3594/T_{cf} + 0.00044T_{cf} - 2.98\log_{10}(T_{cf}), \tag{3}$$

where P is in torr and T_{cf} is the chilling finger temperature in degrees Kelvin, therefore, the internal pressure is controlled via the chilling finger temperature. The source was operated between $-15°$ C and $+5°$ C (6.4 – 52 mTorr) for this work.

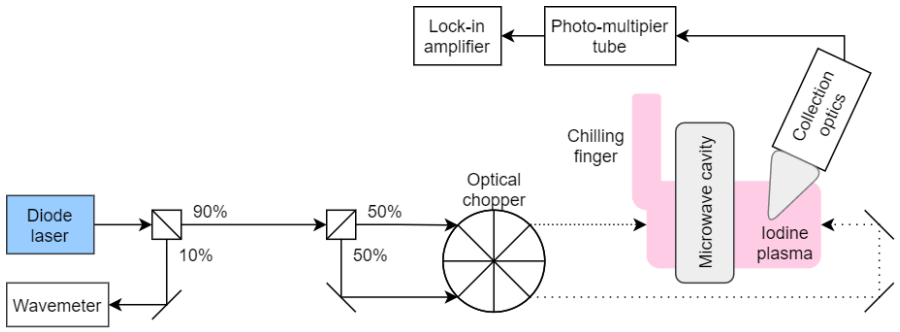

Figure 2: Diagram of the experimental apparatus. A diode laser beam tuned to 696.0694 nm is monitored with a wavelength meter, and sent through a beam splitter which allows two equal components of the beam to be modulated at differing frequencies. The modulated beams are sent antiparallel along the mechanical axis of the quartz iodine cell, exciting particles at rest and emitting light which is collected and filtered as LIF signal. The microwave cavity shown is driven at 2.45 GHz and used to maintain the source plasma. The chilling finger is a part of the cell, and is used to regulate the plasma partial pressure according to Eq. 3.

A Toptica Photonics DL pro single-mode diode laser was tuned to the transition wavelength and split such that 10% of the beam was directed into a Wavemeter WA-1500 laser wavelength meter for wavelength monitoring. The wavelength meter has an accuracy of ± 0.1 pm.[18] The remaining 90% of the beam is coupled to a $\varnothing 5$ μm single mode fiber optic cable and passed through a second beam splitter, sending two 50% beam components through a chopper with two slightly different fin spacings. The two beams are modulated such that their sum frequency is 7.1kHz. The beams are then redirected into the source antiparallel along the mechanical ($\hat{z}$-) axis of the cell. Light emitted from the cell was captured by a set of collection optics and a $\varnothing 1$ mm multi-mode fiber optic cable. Collected light is amplified by a Hamamatsu HC120-05MOD photomultiplier tube. Spontaneous emission is distinguished from the desired LIF emission using a Stanford Research SR830 lock-in amplifier referenced to the sum of the two chopping frequencies.

4. Results

4.1. Intermodulated LIF Measurements

Figure 3 shows a side by side view of typical I II lineshape measurements performed with traditional LIF and intermodulated LIF. Both were measured from the same plasma source. For the traditional LIF measurement (a), the source was operated at 52 mTorr with a time-averaged laser power of 1.44 mW; for the intermodulated measurement (b), the source was operated at 6.4 mTorr with time-averaged laser powers of 2.3 and 2.2 mW. While the presence of a hyperfine structure is evident with traditional LIF, the intermodulated LIF measurement yields a cleaner lineshape.

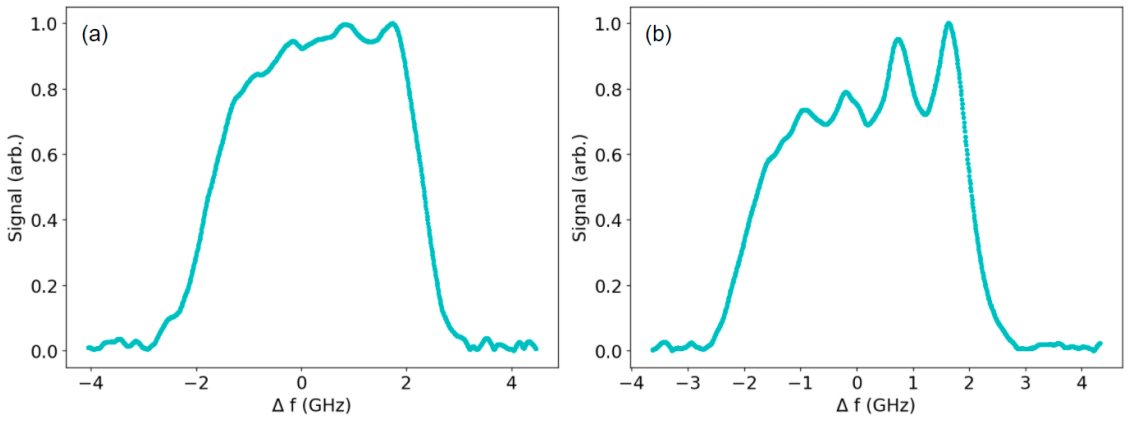

Figure 3: Side by side comparison of a typical I II lineshape measured with traditional LIF (left) and the intermodulated technique (right) described in Section 3. While a hyperfine structure of the observed transition is apparent in the left plot, the use of an intermodulated LIF technique has effectively reduced Doppler broadening to allow for enhanced resolution of the hyperfine structure in the right plot.

4.2. Monte Carlo Fitting

The numerical value of each transition, $\Delta\nu_{hf,i}$ in Table 2, represents the shift, in GHz, from the rest transition frequency. We assume the two highest-intensity frequency shifts can be found within the two most prominent peaks of the lineshape in Fig. 3. Then, values for $\Delta\nu_{hf,1}$ and $\Delta\nu_{hf,2}$ are taken to lie within a ± 0.5 GHz window around the frequency value of these peaks, respectively. This assumption allows the first two equations in Table 2 to be rearranged to solve for A_U and A_L in terms of B_U, B_L, $\Delta\nu_{hf,1}$, and $\Delta\nu_{hf,2}$. Finally, the remaining 13 frequency shift equations are rearranged so that they are only functions of B_U, B_L, $\Delta\nu_{hf,1}$, and $\Delta\nu_{hf,2}$. This approach applies heavier restrictions to possible solutions for the coupling coefficients for these states.

A least-squares fit of Eq. 2, rearranged as described above, to experimental data, yields 21 possible values for each of the free parameters which characterize the measured I II lineshape. Fits are performed iteratively using the function `curve_fit()` from the SciPy Optimize library for Python 3.7.[19] A Monte Carlo fitting algorithm is employed

Transition ($F_L \rightarrow F_U$)	$\Delta\nu_{hf,i}(A_U,\, B_U,\, A_L,\, B_L)$	Relative Intensity
$13/2 \rightarrow 11/2$	$\Delta\nu_{hf,1} = 7.5A_U + 0.25B_U - 10A_L - 0.25B_L$	100
$11/2 \rightarrow 9/2$	$\Delta\nu_{hf,2} = 2A_U - 0.3B_U - 3.5A_L + 0.2375B_L$	76
$9/2 \rightarrow 7/2$	$\Delta\nu_{hf,3} = -2.5A_U - 0.3B_U + 2A_L + 0.29643B_L$	56
$7/2 \rightarrow 5/2$	$\Delta\nu_{hf,4} = -6A_U - 0.02B_U + 6.5A_L + 0.10357B_L$	40
$3/2 \rightarrow 1/2$	$\Delta\nu_{hf,5} = -10A_U + 0.6B_U + 12.5A_L - 0.49107B_L$	18
$7/2 \rightarrow 7/2$	$\Delta\nu_{hf,6} = -2.5A_U - 0.3B_U + 6.5A_L + 0.10357B_L$	16
$9/2 \rightarrow 9/2$	$\Delta\nu_{hf,7} = 2A_U - 0.3B_U + 2A_L + 0.29643B_L$	15
$5/2 \rightarrow 5/2$	$\Delta\nu_{hf,8} = -6A_U - 0.02B_U + 10A_L - 0.19643B_L$	14
$11/2 \rightarrow 11/2$	$\Delta\nu_{hf,9} = 7.5A_U + 0.25B_U - 3.5A_L + 0.2375B_L$	10
$3/2 \rightarrow 3/2$	$\Delta\nu_{hf,10} = -8.5A_U + 0.330B_U + 12.5A_L - 0.49107B_L$	9
$5/2 \rightarrow 3/2$	$\Delta\nu_{hf,11} = -8.5A_U + 0.330B_U + 10A_L - 0.19643B_L$	8
$9/2 \rightarrow 11/2$	$\Delta\nu_{hf,12} = 7.5A_U + 0.25B_U + 2A_L + 0.29643B_L$	1
$7/2 \rightarrow 9/2$	$\Delta\nu_{hf,13} = 2A_U - 0.3B_U + 6.5A_L + 0.10357B_L$	1
$5/2 \rightarrow 7/2$	$\Delta\nu_{hf,14} = -2.5A_U - 0.3B_U + 10A_L - 0.19643B_L$	1
$3/2 \rightarrow 5/2$	$\Delta\nu_{hf,15} = -6A_U - 0.02B_U + 12.5A_L - 0.49107B_L$	1

Table 2: Table of allowed hyperfine transitions between the lower $^5D_4^0$ and upper $^5P_3$ states. The frequency difference between the lower and upper hyperfine state in each transition is given by $\Delta\nu_{hf,i}$ in terms of the coupling coefficients, generating a system of 15 equations and 4 unknown quantities.

here by passing constrained, pseudo-random initial values into `curve_fit()` as initial guesses for each parameter. The signal values are normalized, and the initial signal offset guess is generated between 0 and 0.1, in arbitrary units; the temperature guess is generated between 0 and 1 eV; and the amplitude guesses are generated between 0 and the maximum signal value (between 0 and 1 for the normalized signal), in arbitrary units. The initial guesses for the coupling coefficients are generated between the minimum and maximum frequency values, in GHz, with $\Delta\nu_{hf,1}$ and $\Delta\nu_{hf,2}$ constrained within the 1 GHz windows mentioned above.

The function will take in the initial guesses and return a one-dimensional NumPy array containing the 21 calculated fit parameters. *MacCallum et al.*[20] describe an "extremely close" fit as having an RMSE cutoff value of 0.01, a "close" fit with a cutoff value of 0.05, and a "mediocre" fit with a cutoff value of 0.08. We use these cutoffs to evaluate the goodness of each fit. Here, it is found that a dominating number of the "extremely close" fits have an RMSE value less than 0.07. Therefore, we impose a stricter condition for "extremely close" fits of RMSE ≤ 0.07.

After calculating 10,000 fits of Eq. (2) with randomized starting parameters, the algorithm found 184 "extremely close" fits. The most likely value for the source effective temperature T is 0.0363 ± 0.0021 eV. Most probable values for the $^5P_3$ coupling coefficients A_U and B_U are listed with the most probable values for the $^5D_4^9$ coupling coefficients A_L and B_L in Table 3. The parameters calculated for the 184 "extremely

Coupling Coefficient	Estimated Value (MHz)
A_U	309.9±76.2
B_U	-265.0±100.6
A_L	75.5±54.2
B_L	-441.7±70.7

Table 3: Most probable values for the magnetic dipole and electric quadrupole coupling coefficients of the $^5D_4^0$ and $^5P_3$ hyperfine transitions of singly-ionized atomic iodine.

close" fits were averaged and used to generate the fit depicted in Fig. 4, with the likely locations of each hyperfine transition indicated by the 15 black vertical lines (with error bars) throughout the lineshape.

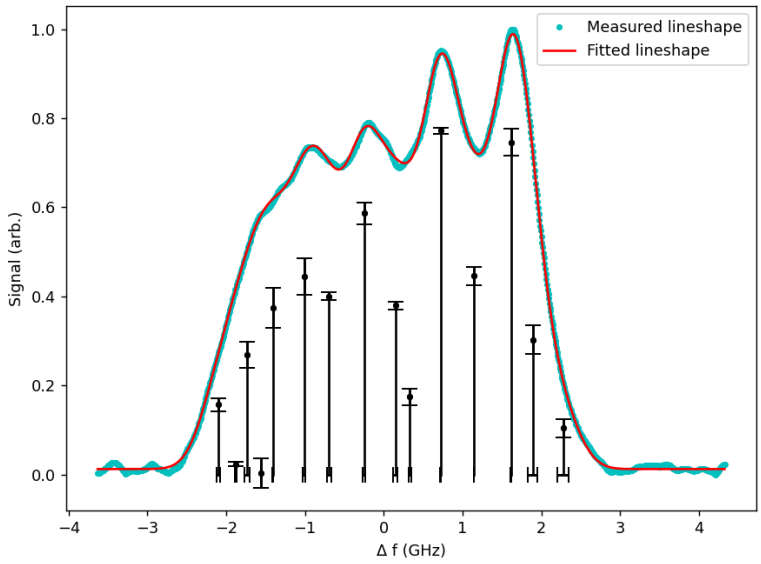

Figure 4: Plot of the measured line shape in blue (dots) with the "best" fit over top of it in red (solid line), calculated with the averages of the parameters from the 184 "extremely close" fits. The black vertical lines show predicted locations of each hyperfine transition, with error bars along both the signal and frequency axes.

5. Conclusions

An intermodulated laser induced fluorescence technique is demonstrated to resolve a Doppler-reudced lineshape of sinlgy-ionized atomic iodine within a microwave plasma discharge. The hyperfine structure of the $^5D_4^0$ and $^5P_3$ states is analyzed, and likely values for the magnetic dipole and electric quadrupole coupling coefficients are reported in Table 3. The likely effective ion temperature of the source is found to be 0.0363±0.0021 eV.

6. Acknowledgements

The authors would like to thank William A. Hargus, Jr., of the Edwards Air Force Research Laboratory, as well as Dr. William Amatucci, and the Naval Research Laboratory for providing several key pieces of the experimental apparatus for this work. We would additionally like to thank Mitchell Paul and Dr. Peiyun Shi for technical consultations. This work was supported by the West Virginia University Center for KINETIC Plasma Physics.

References

[1] Szabo J, Robin M, Paital S, Pote B, Hruby V and Freeman C 2013 Proceedings of the 33rd International Electric Propulsion Conference

[2] Hofer R R and Jacobson D 2004 Development and characterization of high efficiency, high-specific impulse xenon hall thrusters NASA Glenn Research Center 2-59 report number NASA/CR-2004-213099

[3] Dressler R, Chiu Y H and Levandier D J 2000 38th Aerospace Sciences Meeting and Exhibit AIAA Paper 2000-0602

[4] Szabo J, Pote B, Paital S, Robin M, Hiller A, Branam R D and Huffmanm R E 2012 Journal of Propulsion and Power **28** 848–857

[5] Linnell J A and Gallimore A D 2006 Journal of Propulsion and Power **22** 1402–1418

[6] Jacobson D and Manzella D 2003 39th AIAA/ASME/ASEE Joint Propulsion Conference and Exhibit AIAA Paper 2003-4550

[7] Tverdokhlebov O and Semenkin A 2001 37th Joint Propulsion Conference and Exhibit AIAA Paper 2001-3350

[8] Hargus W, Lubkeman J, Remy K and Gonzales A 2012 48th AIAA/ASME/SAE/ASEE Joint Propulsion Conference and Exhibit

[9] Duchemin O, Valentian D and Cornu N 2009 Proceedings of the 45th Joint Propulsion Conference and Exhibit AIAA Paper 2009-4912

[10] Hiller A C 2011 Revolutionizing space propulsion through the characterization of iodine as fuel for Hall-effect thrusters Master's thesis Air Force Institute of Technology, Wright-Patterson AFB

[11] Lide D R 2004 CRC Handbook of Chemistry and Physics 84th ed (CRC Press, Boca Raton, FL)

[12] Dorf L, Raistes Y and Fisch N J 2004 Review of Scientific Instruments **75** 1255–1260

[13] Steinberger T and Scime E 2018 Journal of Propulsion and Power **34** 1235–1239

[14] Stern R A and Johnson J A I 1975 Physical Review Letters **34**

[15] McIntyre D H 2012 Quantum Mechanics: A Paradigms Approach 2nd ed (Pearson Addison-Wesley) ISBN 978-0-321-76579-6

[16] Sorem M S and Schawlow A L 1972 Optics Communications **5** 148–151

[17] Kono A and Hattori S 1979 Journal of the Optical Society of America **69** 253–255

[18] Inc E E O E 2004 Use Guide: WA-1000/WA-1500 Wavemeter Laser Wavelength Meters

[19] Bell P, Burovski E, Casey C J, Gommers R, Larsen P M, Lee C H, Ma C, McKibben N, Forro N, Reddy T and Weckesser W 2021 Scipy 1.6.1 https://docs.scipy.org/doc/scipy/reference/index.html, accessed Apr. 1, 2021

[20] MacCallum R C, Browne M W and Sugawara H M 1996 Psychological Methods **1** 130–149

[21] Hall E H 1879 American Journal of Mathematics **2** 287–292

[22] White H E 1934 Introduction to Atomic Spectra (McGraw-Hill, New York)